Redox Biology 78 (2024) 103398

Contents lists available at ScienceDirect

Redox Biology

journal homepage: www.elsevier.com/locate/redox

Metabolic stress in space: ROS-induced mutations in mice hint at a new path to cancer

Viktor Stolc [a,*], Miloslav Karhanek [b], Friedemann Freund [c], Yuri Griko [a], David J. Loftus [a], Maurice M. Ohayon [d]

[a] NASA Ames Research Center, Moffett Field, CA, 94035, USA
[b] Biomedical Research Center, Slovak Academy of Sciences, 845 05, Bratislava, Slovakia
[c] SETI Institute, Mountain View, CA, USA
[d] Stanford University, School of Medicine, Stanford, CA, 94305, USA

A B S T R A C T

Long-duration spaceflight beyond Earth's magnetosphere poses serious health risks, including muscle atrophy, bone loss, liver and kidney damage, and the Spaceflight-Associated Neuro-ocular Syndrome (SANS). RNA-seq of mice aboard the International Space Station (ISS) for 37 days revealed extraordinary hypermutation in tissue-specific genes, with guanine base conversion predominating, potentially contributing to spaceflight-associated health risks. Our results suggest that the genome-wide accelerated mutation that we measured, seemingly independent of radiation dose, was induced by oxidative damage from higher atmospheric carbon dioxide (CO_2) levels and increased reactive oxygen species (ROS) on the ISS. This accelerated mutation, faster *via* RNA transcription than replication and more numerous than by radiation alone, unveils novel hotspots in the mammalian proteome. Notably, these hotspots correlate with commonly mutated genes across various human cancers, highlighting the ISS as a crucial platform for studying accelerated mutation, genome instability, and the induction of disease-causing mutations in model organisms. Our results suggest that metabolic processes can contribute to somatic mutation, and thus may play a role in the development of cancer. A metabolic link to genetic instability potentially has far-reaching implications for various diseases, with implications for human health on Earth and in space.

1. Introduction

There is growing appreciation that subtle changes in the genome may have an impact on human health and disease [1]. Single nucleotide polymorphisms (SNPs), for example, may be relevant to some spaceflight-induced health risks, which include radiation susceptibility, changes in bone density, muscle loss and drug metabolism [2]. Somatic mutations – also called single nucleotide variants (SNVs) or single base substitutions (SBSs) – low frequency post-zygotic somatic mutations leading to somatic mosaicism—are another type of genetic alteration that could impact space physiology as well [3]. Next Generation Sequencing (NGS) data (from RNA-Seq data) from animals flown to the International Space Station (ISS) have become available to enable analysis of somatic mutation which may shed light on this fundamental genetic process that occurs across species that may have clinical relevance for astronauts.

A wide range of physiological changes occur in astronauts during spaceflight, many of which can be attributed to the physiological effects of weightlessness [4]. Acute changes include a headward redistribution of blood volume, resulting in a puffy face and fullness of the upper torso. Over time, there is a net reduction in total blood volume and a reduction in red cell mass. Weightlessness is associated with decreased mechanical loading of the skeleton and reduction in bone calcium, as well as muscle atrophy. Weightlessness and fluid redistribution are associated with swelling in the back of the eye (Spaceflight-Associated Neuro-ocular Syndrome (SANS). Other changes include disruption of inner ear function, termed space motion sickness. An additional stressor of spaceflight is space radiation, which will become significant as astronauts embark on deep space missions. Current missions to the ISS do not expose space travelers to significant space radiation because of the protection provided by the Earth's magnetosphere.

While spaceflight induced changes in humans can be explained by physics and physiology, at least in part, there has been little attention paid to the topic of somatic mutation (single nucleotide variants—SNVs), which may contribute to alterations in the biology of mammalian systems *via* changes in the proteome and may affect the ability of individuals to adapt to space.

We report, herein, the first study of somatic mutation in mice in Low Earth Orbit, a space environment where radiation is not a major factor. This study was made possible by the availability of gene expression data

* Corresponding author.
E-mail address: viktor.stolc-1@nasa.gov (V. Stolc).

https://doi.org/10.1016/j.redox.2024.103398
Received 2 October 2024; Accepted 14 October 2024
Available online 16 October 2024

from validation experiments involving mice that spent 5–6 weeks on the ISS. While many forms of genetic analysis have been applied to the study of model organisms in space [5], including gene expression studies, DNA methylation studies, RNA methylation studies, proteomics, and metabolomics (in humans, in model organisms and even in plants) [6], this is the first study that looks specifically at the topic of somatic mutation. In the biomedical literature, most studies of somatic mutation are focused on the genomic changes that accompany the development of cancer [3]. This study is more broadly framed, consisting of an examination of somatic mutations in normal tissues. Findings presented here may have implications for degenerative diseases and inflammatory conditions associated with spaceflight, in addition to carcinogenesis. This investigation opens a whole new arena of scientific inquiry that may lead to better understanding of the health risks of spaceflight.

2. Material and methods

2.1. Protocol

A cohort of 18-week-old female BALB/c and C57BL/6J mice were flown to the ISS and housed in the Rodent Habitat and were subjected to microgravity for 37 days. Mice of similar age, sex and the same strain were used for ground controls housed in identical hardware and simulating, but not exactly matching ISS environmental conditions (i.e., simulating temperature, humidity, and gas atmosphere). Notably, the ISS displayed the highest $PaCO_2$ compared to ground controls, exhibiting an average fractional deviation of 0.08 during spaceflight, along with a transient 40 % increase for 1.5 h (telemetry data not shown). In contrast, vivarium mice were housed in the Earth's ambient atmosphere. Mice from the same cohort were dissected at time of launch and used as basal controls. At the end of the mission, spaceflight and ground controls were euthanized and whole carcasses were stored at −80°C until BSP (Biospecimen Sharing Program) dissection on earth. Tissues of BALB/c and C57Bl/6J mice were dissected and preserved at various time points post-euthanasia and stored at −80 °C for up to 11 months. In some experiments, tissues were recovered from frozen carcasses which had been stored at −80 °C for up to 7 months. RNA quantity and quality were assessed by measuring RNA Integrity Number (RIN) values using an Agilent Bioanalyzer. Additionally, the quality of tissues was assessed by measuring activities of hepatic enzymes (catalase, glutathione reductase and GAPDH).

2.2. Samples

Mouse carcasses were removed from −80°C storage and thawed at room temperature for 15–20 min for dissection. Each carcass dissection time was no longer than 1 h from collection of the first tissue. Multiple tissues, including the eye, quadriceps muscle, kidney, and liver tissues, were collected from each carcass. Tissues were harvested and snap frozen in liquid nitrogen, then stored separately in −80 °C freezer for sample processing. GeneLab Sample Processing Lab processed all tissues from spaceflight, ground control, and basal control groups for transcriptomics.

2.3. Nucleic acid sequencing

RNA sequencing performed on Illumina HiSeq 4000. Paired end, 150bp. DNA sequencing performed on Illumina HiSeq 4000. Single-end read, 150bp. Performed by UC Davis Genome Center.

2.4. Nucleic acid extraction

RNA was extracted using the AllPrep DNA/RNA Mini Kit (Qiagen, Valencia, CA). Briefly, homogenization buffer for RNA purification was made by adding 1:100 vol of beta-mercaptoethanol to Buffer RLT (Qiagen, Valencia, CA) and kept on ice until use. Tissues were immediately placed in 600 μL of the Buffer RLT solution. Each sample was then homogenized for approximately 20 s at 21,000 RPM using a Polytron PT1300D handheld homogenizer with a 5 mm standard dispersing aggregate tip (Kinematica, Bohemia, NY). Homogenates were centrifuged for 3 min at room temperature at 21,300 g to remove cell debris. Following the manufacturer protocol, RNA was isolated and purified from the supernatant. RNA was eluted in 40 μL RNase-free H_2O and concentration measured using Qubit 3.0 Fluorometer (Thermo Fisher Scientific, Waltham, MA). RNA quality was assessed using the Agilent 2100 Bioanalyzer with the Agilent RNA 6000 Nano Kit or Agilent RNA 6000 Pico Kit (Agilent Technologies, Santa Clara, CA).

2.5. RNA sequencing data processing protocol

All single nucleotide variants (SNVs) were identified against the Genome Reference Consortium Mouse Build 38, GRCm38 in eye, kidney, quad muscle, and liver tissues using the GATK and MuTect, which are accurate and reliable methods for identifying somatic point mutations in next generation sequencing (NGS) data. The used pipeline was tested by tools and data downloaded from the precision FDA website, showing variant calling precision 98.31 % and sensitivity 99.30 % for SNVs calling [7–9]. Approximately 5 Tb of deep RNA sequencing data from the NASA GeneLab database [https://genelab.nasa.gov/] were used at up to 10x sequencing depth coverage per tissue sample. The set included 472 transcriptomes and compared 236 flight and 236 ground samples with 71 sample pairs, *i.e.*, 142 samples per tissue (except 24 sample-pairs for liver tissue, *i.e.*, 48 samples for liver). The selection criteria for inclusion of sequence variants in mutations versus expressions analysis (Fig. 5A–D) required that single-nucleotide variant (SNV), each *de novo* induced during spaceflight, had to be present in at least 20 % of the samples for each included gene.

2.6. Somatic mutation calling

Somatic mutations were called using GATK MuTect2 pipeline. Briefly, somatic SNVs were called from flight samples using its corresponding ground as control. First, calling was performed by GATK Haplotypecaller for each flight and ground samples separately. Low quality SNVs calls from Haplotypecaller were filtered out. For MuTect2, aligned bam file of flight sample was input as 'tumor' and ground control sample as 'normal'. The reference genome was included in its input parameters and all other parameters were set as default. SNVs identified as 'Novel' and passed default filters by MuTect2 with minimum sequencing depth of 20 in both flight and ground sample were used for further filtration.

The final vcf files were then annotated by Annovar [10] and analysed by VEP (Variant Effect Predictor from Ensemble) *via* the Ensembl Representational State Transfer (REST) application program interface (API) [11]. The results from all files were then accumulated and summarized by in-house Python scripts and processed by Excel Visual Basic for graph presentations. Filtering out of variant artifacts was performed for controls (ground samples) when ALT/REF ratio exceeded 9 %. On the other hand, flight variants were removed when ALT/REF was less than 2 %. This ensured avoidance of spurious ALTs in both sample groups. All samples from all tissues were treated with the same filtering protocol.

2.7. Differential expression analysis (DEA)

For differential expression analysis (DEA), TPM (Transcripts Per Million) values gathered by Kallisto [12] were used to consider the distribution of transcript lengths in the samples and thus quantify RNA transcript amounts consistently between samples [13]. For DEA, we first used median of ratios normalization method, followed by Standard Student's t-test calculation of P-values for each gene in both groups *i.e.*, flight *vs* ground. Statistical significance was considered at $P < 0.05$ in follow-up bioinformatics analyses.

2.8. Calculation of mutation frequency

For the calculation of mutation frequency (number of mutations per base pair) we used a calculation as previously described [14]. It is assumed that each mutation reflects an independent event that has a small probability of occurring and has an infinitesimal probability of occurring twice at the same position. Thus, each base pair could be considered an independent Bernoulli trial with an output of either mutated or not mutated and the average number of mutations in a gene could be calculated by the zero order of the Poisson process. The average frequency of mutations (N0/N, where N0 is the number of unaltered positions and N the total number of bases sequenced) thus equals $e^{-\lambda}$ and from this $\lambda = -\ln(N0/N)$, where λ represents the average number of mutations per base pair, *i.e.*, frequency of mutation.

2.8.1. Data availability

RNA-seq data generated in this study are deposited to the NASA GeneLab database [https://genelab.nasa.gov/]. All analyses were conducted using standard software. The settings of software used for analyses are described in the Methods. Source data are provided with this paper.

2.8.2. Source data

GLDS-102**:** Rodent Research-1 (RR1) NASA Validation Flight: Mouse kidney transcriptomic, proteomic, and epigenomic data.

GLDS-103: Rodent Research-1 (RR1) NASA Validation Flight: Mouse quadriceps muscle transcriptomic, proteomic, and epigenomic data.

GLDS-137**:** Rodent Research-3-CASIS: Mouse liver transcriptomic, proteomic, and epigenomic data.

GLDS-162: Rodent Research-3-CASIS: Mouse eye transcriptomic and proteomic data.

3. Results

3.1. Spaceflight induced tissue specific mutations in mice

A high precision variant calling pipeline using GATK and MuTect [7,10,11], which has previously been shown to be appropriate for variant analysis of RNA-Seq data [15–17], was used to identify and map the chromosomal coordinates for all somatic mutations from RNA-Seq data of 18-week-old female BALB/c and C57BL/6J mice that were flown for a short period of time (5–6 weeks) on the ISS. This was done by comparing ISS flight animals to simultaneous ground controls animals housed in the same habitats and in ambient vivarium. The computational analysis was done for each corresponding pair of RNA data sets (Supplementary Tables 1–8), using the NASA GeneLab Data Systems files referenced in the Source Data. All somatic mutation determinations were performed using the reference genome GRCm38, which is a composite of multiple strains, including the BALB/c and C57BL/6J strains [18]. Combining results from all tissues examined–eye, kidney, liver and skeletal muscle (quadriceps muscle)—we observed an exonic mutation frequency of 5.55×10^{-6} per base pair (bp) for all differentially expressed genes for mice on board the ISS, as compared to the previously established value of 5.3×10^{-9} mutations per bp (1.7 mutations per genome per generation) [18,19], which is well-established for mice. Data from a total 18140 genes with expressions in at least 3 samples in each ground and ISS mouse tissue (see Supplementary Tables 5–8) was identified in the experimental animals that were flown in space. For any multicellular organism, this represents an exceptionally high genome-wide "hypermutation rate." Interestingly, the average exonic mutation frequency of 6.69×10^{-6} per bp on the ISS relative to the value for ground controls 3.79×10^{-7} was identified in genes that were significantly differentially expressed on the ISS (total 3520 genes, P-value <0.05), which is about 18 times higher average mutation frequency on the ISS. Exonic mutation frequency for all mutated genes (18140 genes) was about 27 times higher on the ISS. This result shows that there is a higher mutation frequency in genes transcribed on the ISS.

Fig. 1 shows the statistical distribution of somatic mutation rates for each of the four tissue types examined in this study. Table 1A shows a summary of identified genes for each tissue and calculations of average frequency of mutation per bp. The lowest average frequency of somatic mutation was seen in the kidney and skeletal muscle (5.30e-6, 5.40e-6, respectively) but these values, nonetheless, represent substantial hypermutation. Liver and eye tissues showed the highest average rate of somatic mutation (6.87e-6 and 7.89e-6), with eye about 1.3–1.5 times higher than kidney and skeletal muscle. Published studies for humans indicate that the rate of somatic mutation is tissue-specific (with somatic mutation rate for liver reported as being higher than that for skeletal muscle) [20], but no such study in mice has previously been reported. Few studies of somatic mutation in eye tissue exist in any species. Table 1B shows a summary of differentially expressed genes that met significance (P-value <0.05) and the calculated mutation frequencies for tissues in exons on the ISS, ground, and vivarium. The mutation frequency exhibited a consistent pattern, with approximately 6–7 times higher rates on the ISS compared to ground controls across individual mouse tissues, except for eye tissue where it was about 17.5 times higher. The findings reveal distinct mutation rates in different tissues, which we hypothesize may be attributable to variations in reactive oxygen species (ROS) stemming from tissue-specific metabolic rates. These findings also implicate elevated CO_2 levels on the ISS, relative to ground controls (in which simulated ISS CO_2 levels were targeted) and vivarium controls (with Earth's ambient CO_2 levels), in conjunction possibly with other spaceflight factors, as contributing to heightened somatic mutation. The relationship between CO_2 and somatic rate is discussed in more detail below.

Fig. 2 provides an easy visualization of the numbers of mutated genes that are unique to the four tissue types examined, as well as mutated genes in common between the various tissues. The overlapping zones of

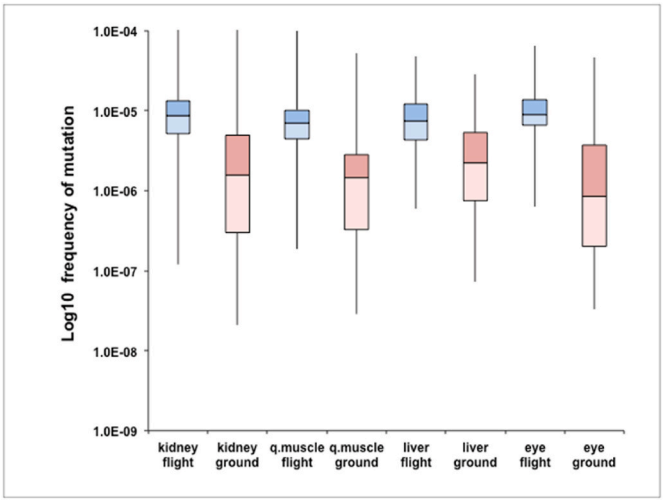

Fig. 1. Box plot graph of statistical distribution of the average number of mutations per base pair (mutation frequency) for different mouse tissues on the ISS (blue) relative to ground controls. Medians (bar between dark blue and light boxes) for kidney, quad muscle, liver, and eye tissues are 8.63e-6, 7.11e-6, 7.47e-6 and 8.92e-6, respectively. Box lengths correspond to the interquartile range (IQR) representing values between 75th and 25th percentiles. The frequency values were calculated for the significantly induced genes exhibiting mutations in at least 20 % of samples (with a P-value <0.05) with exonic mutations for different tissues (kidney: 171 genes, quad muscle: 237 genes, liver: 246 genes, eye: 364 genes). Medians for ground controls kidney, quad muscle, liver, and eye are 1.58e-6, 1.45e-6, 2.23e-6 and 8.50e-7 for the related number of mutated genes 151, 171, 166 and 223 respectively. (Non-mutated ground genes cannot be displayed due to boxplot limitation collapsing when values are 0). Supplementary Tables 5A–8A contain all values used for the statistical calculation.

Table 1A
Summary of found differentially expressed genes and calculated mutation frequencies for all tissues and all samples on the ISS. Frequency calculations were performed according to Balin [14].

Tissue	Number of differentially expressed genes	Number of significantly differentially expressed genes ($p < 0.05$)	Mutation frequencies for all differentially expressed genes	Mutation frequencies for significantly differentially expressed genes
GLDS-137 (liver)	4234	430	6.69E-06	6.87E-06
GLDS-162 (eye)	7149	1683	6.18E-06	7.89E-06
GLDS-102 (kidney)	3842	786	4.41E-06	5.30E-06
GLDS-103 (quad muscle)	2915	621	4.97E-06	5.40E-06
Total	**18140**	**3520**	**5.55E-06**	**6.69E-06**

Table 1B
Summary of identified significantly differentially expressed genes (P-value <0.05) and calculated mutation frequencies for tissues in exons on the ISS, ground and vivarium. The frequency values were calculated for the significantly expressed genes exhibiting mutations in at least 20 % of samples.

Tissue	Group (Mutect2)	Number of significantly differentially expressed genes with exonic mutations ($p < 0.05$)	Mutation frequencies for significantly differentially expressed genes	Fold change
GLDS-137 (liver)	ground/ vivarium	312/305	1.27E-05/2.47E-06	5.14
GLDS-137 (liver)	flight/ground	274/168	7.24E-06/1.18E-06	6.13
GLDS-137 (liver)	flight/ vivarium	866/503	2.54E-05/2.57E-06	9.91
GLDS-162 (eye)	ground/ vivarium	305/164	1.12E-05/1.62E-06	6.94
GLDS-162 (eye)	flight/ground	558/298	8.44E-06/4.83E-07	17.48
GLDS-162 (eye)	flight/ vivarium	410/206	1.34E-05/1.25E-06	10.71
GLDS-102 (kidney)	flight/ground	267/210	7.03E-06/9.87E-07	7.12
GLDS-103 (quad muscle)	flight/ground	278/189	6.24E-06/8.93E-07	6.99

the Venn diagram represent comparison in a pairwise fashion (6 comparisons), comparison amongst three tissue types (4 comparisons), and comparison amongst four tissue types (1). Overall, most mutated genes were specific to the individual tissue types studied; there was little overlap. Only a single gene (Eukaryotic Translation Elongation Factor 2) was mutated across all four types of tissue.

The Venn diagram in Fig. 3 shows the number of total numbers of somatic mutations within the mutated genes, with the data organized according to tissue type. In addition to exhibiting the greatest number of induced and mutated genes by spaceflight (data shown in Fig. 2), the eye exhibited the greatest total number of somatic mutations, with multiple somatic mutations for many genes (Fig. 3).

The Venn diagram in Fig. 4 shows the number of tissue specific genes mutated with non-synonymous mutations on the ISS relative to ground controls.

To address the question *Does the extent of somatic mutation in spaceflight correlate with the degree of gene expression?* the protein coding genes were categorized according to degree of gene expression, establishing four quartiles, Q4: 75–100 % (highest quartile of gene expression), Q3: 50–75 %, Q2: 25–50 %, Q1: 0–25 % (lowest quartile of gene expression). RNA transcript levels were normalized as transcripts per million (tpm), *i.e.*, we used a scaling factor, which means that for every 1,000,000 RNA molecules in the RNA-sequence sample, x came from a particular gene/transcript. The selection criteria for inclusion of sequence variants required that single-nucleotide variant (SNV) had to be present in at least 20 % of the samples for each gene. A statistically significant relationship was identified between gene mutations expressed as SNVs for different tissues, with 920 unique SNVs per sample in eye tissue from BALB/c mice (GLDS-162), 421 unique SNVs per sample in kidney tissue from C57BL/6J mice (GLDS-102), 494 unique SNVs per sample in quad muscle from C57BL/6J mice (GLDS-103), and 1114 unique SNVs per sample in liver tissue from BALB/c mice (GLDS-137), and spaceflight induced RNA expression levels divided into four quartiles of gene expression, Q4: 75–100 %, Q3: 50–75 %, Q2: 25–50 %, Q1: 0–25 %. The results are shown in Fig. 5A–D. For each of the four tissue types, somatic mutation rate was highest for the top two quartile of gene expression, except eye, where somatic mutation rate was highest in just the top quartile. The significant increase of spaceflight mutation frequency *versus* ground was confirmed with P-values <0.05 for all gene expression quartiles in all tissues. The frequency values were calculated again (see Fig. 1) for significantly induced genes exhibiting mutations in at least 20 % of samples.

Remarkably, some of the ISS induced unique SNVs were present in greater than 50 % of the sequenced traces per tissue samples, and represent 10.5 %, 6.2 %, 9 %, 7.3 % of all SNVs in eye, kidney, quad muscle, and liver tissue, respectively (Supplementary Tables 1–4). Another remarkable result is that the ground control mice, which were also exposed to elevated CO_2 levels, showed a rate of somatic mutation accumulation that was intermediate between the mice flown on the ISS and what was identified for ground control mice (known as the baseline, BSL, or vivarium samples) in the absence of excess CO_2 exposure (Fig. 5 and Table 1B).

To shed light on the mechanism of somatic mutation, the relative proportion of each type of somatic mutation base substitution was determined, as shown in Fig. 6. In the experimental animals flown to the ISS, guanine was the most frequently substituted base (Fig. 6, bars 7–9), most often involving conversion to adenine. This result is consistent with adenine being most efficiently inserted when abasic sites are bypassed by DNA polymerases [24]. In fact, adenine was the least substituted base (Fig. 6, bars 1–3) (see Supplementary Table 18). This finding helps to confirm that the guanine substitutions that we did see (inferred from analysis of the RNA-Seq data) were indeed the result of somatic mutations in the DNA, as opposed to changes in RNA due to RNA editing. With RNA editing, we would have expected predominantly A > G conversion, which we did not see Ref. [25]. The substitutions that we inferred from analysis of the RNA-Seq data (Supplementary Table 18) show all the unique relative counts for each SNV, in eye, kidney, liver, and skeletal muscle tissues.

The predominance of guanine base substitution suggests that guanine oxidation may be playing a significant role in the process of somatic

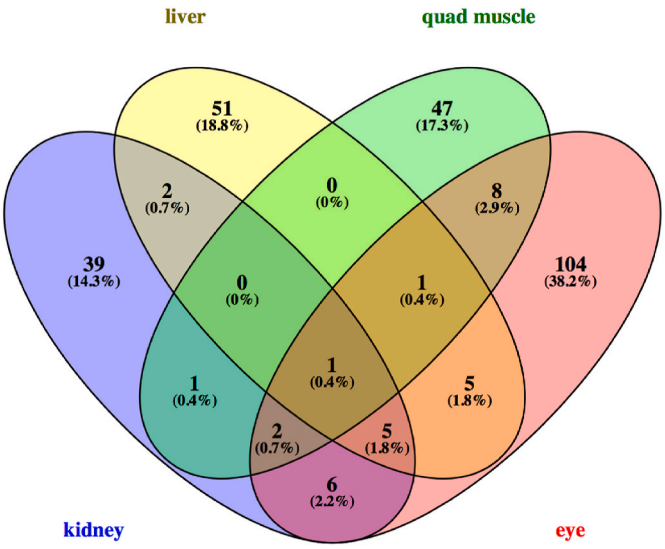

Fig. 2. A Venn diagram showing the number of tissue-specific genes from Tables 1–4 with significantly induced RNA expressions and highest number of mutations per gene on the ISS relative to ground controls. Tissue-specific genes with significantly induced RNA expressions (with a P-value <0.05) on the ISS (39 in kidney, 47 in muscle, 51 in liver, and 104 in eye) that have the highest number of mutations in top expression quartile (>75 %), *i.e.*, at least 15 SNVs per gene in each tissue. One such mutated gene common in all mouse tissues is *EEF2*, encoding the Eukaryotic Translation Elongation Factor 2, which is hypermutated at various positions, including by insertion of adenine at a single, identical position in all tissues, *i.e.*, at chromosome 10, position 81,179,400 in the Genome Reference Consortium Mouse Build 38, GRCm38. The *EEF2* gene also showed variable tissue specific unique number of mutations, *i.e.*, 57 SNVs in eye, 27 SNVs in kidney, 22 SNVs in quad muscle, and 13 SNVs in liver tissues, tracking the total relative unique mutations for the four tissues per sample, *i.e.*, eye > kidney > quad muscle > liver. The human *EEF2* is also a tumor-associated antigen overexpressed in various types of cancers, suggesting susceptibility to hypermutation [21]. Table 9 shows the names of all genes in the Venn diagram.

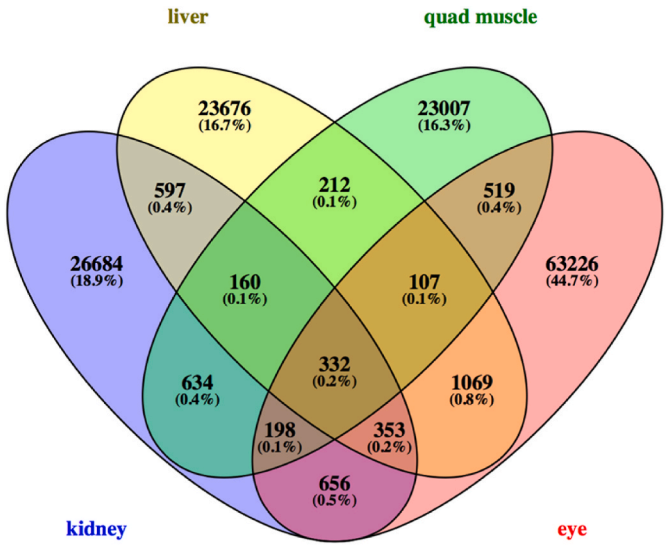

Fig. 3. A Venn diagram showing the number of tissue specific single nucleotide variants (SNVs) from Tables 1–4 that were mutated on the ISS relative to ground controls. Surprisingly, there were 332 genome-wide SNV hotspots in common to all mouse tissues that were mutated on the ISS. The corresponding genes (249) that were mapped to the common SNV hotspots are shown in Table 14. One of the commonly mutated genes is a small RNA, Gm15441, which suppresses its antisense transcript, encoding thioredoxin interacting protein (TXNIP) and multiple mutations in this gene likely increased ROS accumulation in all tissues on the ISS by inhibiting the antioxidative function of thioredoxin (*TXN*). In comparison, deletion of *TXN* increased the mutation rate by 2000 % in microorganisms [22].

mutation on board the ISS. Of all the nucleotide bases, guanine is the most readily oxidized [26,27]. Guanine oxidation may occur because of endogenous production of reactive oxygen species (ROS) inside cells [27]. Cytosine base substitutions were also seen commonly (C > T transitions). Our finding of C > T transitions is consistent with findings in *E. coli* in which the C > T transition *via* an oxidative deamination pathway has been well documented in [28]. Taken together, these results point to ROS being responsible for genome-wide sequence variation during RNA transcription in the oxidative phase of the redox cycle, rather than during DNA replication, which is restricted to the reductive phase when ROS are neutralized [29].

While some of the G-to-A mutations at the DNA level may be corrected by post-transcriptional A-to-I RNA editing, which is the most prevalent type of RNA editing known in the animal kingdom [25,30], the vast majority (about 97 %) of A-to-I editing events occur in the noncoding regions (5′- or 3′-untranslated regions (UTRs) and introns) [31], rather than in the coding sequences (exons) of mRNAs, as mapped in tissue samples on the ISS relative to the ground controls (Supplementary Tables 17 and 19). These results show that guanine is the most oxidized base, likely by carbonate radical ($CO_3^{\bullet-}$) derived from the reaction of CO_2 and ROS, in agreement with guanine having the lowest standard reduction potential of the other three bases [32]. With tissue-specific data in mind, it appears that ROS seem to be produced at the highest relative concentrations in eye, kidney, quad muscle, and liver tissues, respectively. Indeed, the light-sensitive photoreceptors in the retina are, metabolically, extremely demanding and have the highest density of ROS-producing mitochondria of any cell in the body [33], and most mitochondrial diseases exhibit some form of visual impairment [34].

3.2. Hypoxia-associated genomic instability in mice on the ISS

Spaceflight factors on the ISS, such as reduced O_2 and elevated CO_2 may be relevant to some of the known spaceflight health risks, including hypoxia-induced red blood cell membrane fragility that results in hemolysis in astronauts [35]. As hypoxia is strongly associated with mutational density and genome instability in human tumors [36,37], gene mutations previously identified as driver mutations across 1188 tumors spanning 27 cancer types were mapped in SNVs and in non-synonymous mutations (NSMs), *i.e.*, mutations that change the amino acid identity in proteins, induced in mice on the ISS relative to ground controls. ISS-associated mutations were indeed found in 9 out of 10 driver genes common to all human cancers associated with hypoxia (Supplementary Tables 1–4). Specifically, ISS induced mutations in the mouse oncogene *MYC,* tumor suppressors *TP53, PTEN, CREBBP*, *SGK1*, apoptosis inhibitor *BCL2* and in *STAT6*, *VHL, RAF1* were identified, tracking the total relative unique mutations on the ISS relative to ground controls for the four mouse tissues per sample.

As hypoxic cells acquire a mutator phenotype that consists of decreased DNA repair and increased mutation rate [38], these results indicate that hypoxia due to an increased partial pressure of CO_2 ($PaCO_2$) may have caused the increased mutational load on the ISS relative to ground controls. Additionally, cellular response to hypoxia is mainly controlled by the hypoxia-inducible factor 1 (*HIF-1*), which had multiple SNVs and NSMs induced by the ISS environment in each of the four tissues. Mutations in *HIF-1* likely impaired its means of controlling gene expression by changes in oxygen tension [39,40].

Up to 17 % of all genes mutated on the ISS are found in regions of hyperactive chromatin, which encode super active enhancers and promoters of RNA transcription [41]. For example, micro-RNA, Mir5098, encoded in different species of vertebrates by an orthologous region of hyperactive chromatin, was mutated in all mouse tissues on the ISS

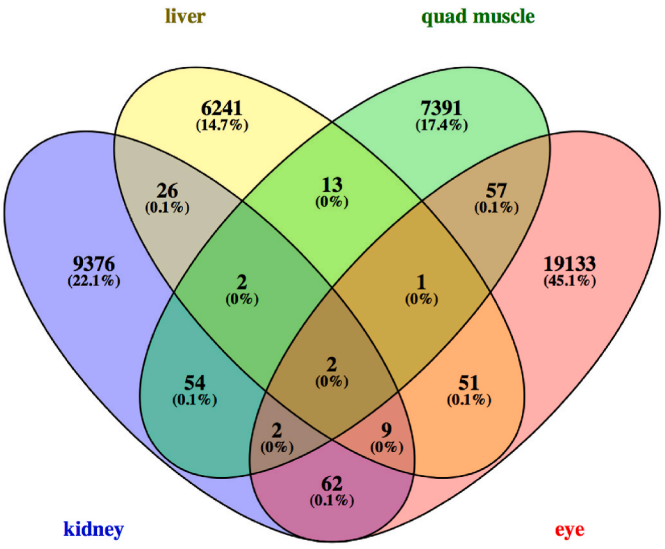

Fig. 4. A Venn diagram showing the number of tissue specific non-synonymous mutations (NSMs), compared as 15-mer peptides with NSM in the middle of the peptide, from Tables 5A–8A shows the number of tissue specific genes mutated on the ISS relative to ground controls. Two NSMs are identical to the common mutated hotspots in all tissues. One of the common hypermutated positions in all tissues was identified in the *SON* gene, which functions in DNA and RNA binding activities involved in promoting efficient splicing of transcripts that possess weak splice sites and is associated in several human health disorders. The second common hypermutated position in all tissues was found in the *NDUFA1* gene [23], which encodes a subunit of NADH dehydrogenase (ubiquinone) with respiratory chain complex I deficiency that presents with highly variable morbidity due to exercise intolerance and muscle wasting and is involved in several human health disorders. The corresponding NSM in *NDUFA1* is a pathogenic mutation that leads to a progressive mitochondrial complex I-specific neurodegenerative disease and a severe muscle defect [23]. All NSMs are listed in Tables 5A–8A

relative to ground controls. Also, miR-21, which is one of the most frequently induced miRNAs in solid tumors and has been experimentally validated as targeting the tumor suppressors *PTEN* and BCL2 [42,43] (found to be mutated in all mouse tissues on the ISS), was identified as one of the most mutated small RNAs by the ISS environment, but not equally in every tissue (Supplementary Tables 1–4). These results indicate that transcriptionally hyperactive regions of the mouse genome are susceptible to tissue specific mutation rates on the ISS.

3.3. Non-synonymous mutations (NSMs) induced by the ISS can pose potential health hazards

The likelihood of having more than one NSM per gene is exceptionally low, approximated by [1/1500 * 2/3]^N, where 1500 denotes the average protein-coding gene length in bases, 2/3 represents the proportion of bases governing distinct amino acids due to the variable base-pairing rules at the third position of each codon, and N signifies the count of NSMs. Interestingly, spaceflight on the ISS induced up to 60, 33, 31, and 23 NSMs per single genes in eye, kidney, quad muscle, and liver tissues, respectively (Supplementary Tables 5–8). The probability of a single gene being mutated randomly at up to 60 NSMs is incredibly small, indicating an environmentally induced rate of mutation previously undescribed for any organism. Most of the mutated genes with multiple NSMs are tissue-specific, with the highest number of NSMs in the eye tissue (Supplementary Tables 5–8). Non-random, genome wide hypermutation is evident in NSMs representing about one third of all SNVs. Additionally, most of the SNVs were tissue-specific, showing significant differences in mutational statistics with a P-value <0.05 for the top three RNA expression quartiles (Q2-Q4) (Supplementary Tables 1–4). There was no significant difference between the Q1 and Q2 quartiles, indicating that the rate of RNA transcription is coupled with the frequency of mutation in mice on the ISS, as was already shown to occur during ROS coupled oscillation of RNA transcription in yeast [29].

SNVs induced by accelerated mutation during spaceflight on the ISS

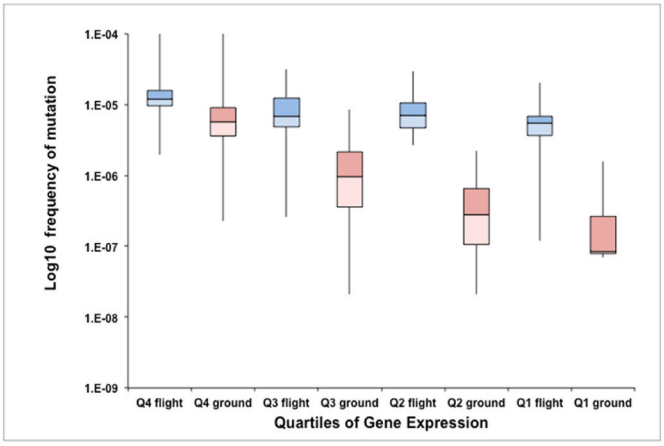

Fig. 5A. Tissue-specific mutation associated with RNA transcription during spaceflight on the ISS relative to ground controls—Kidney. Box plot graph of the statistical distribution of exonic mutation frequency (log10 of frequency of mutation) *vs.* significant differential gene expressions in different gene expression quartiles for GLDS-102 (kidney) samples on the ISS (blue) relative to ground controls (red). The length of each box is the interquartile range (IQR) that represents values between the 75th and 25th percentiles (blue boxes). Medians (bar in between dark blue and light blue boxes) for spaceflight gene expression quartiles Q4, Q3, Q2 and Q1 are 1.21e-5, 6.89e-6, 7.00e-6 and 6.62e-6 for number of genes 56, 57, 39 and 19 respectively. Medians for ground control gene expression quartiles Q4, Q3, Q2 and Q1 are 5.72e-6, 9.63e-7, 2.79e-7 and 8.43e-8 for the related number of mutated genes 56, 51, 33 and 10 respectively. (Non-mutated ground genes cannot be displayed due to boxplot limitation collapsing when values are 0).

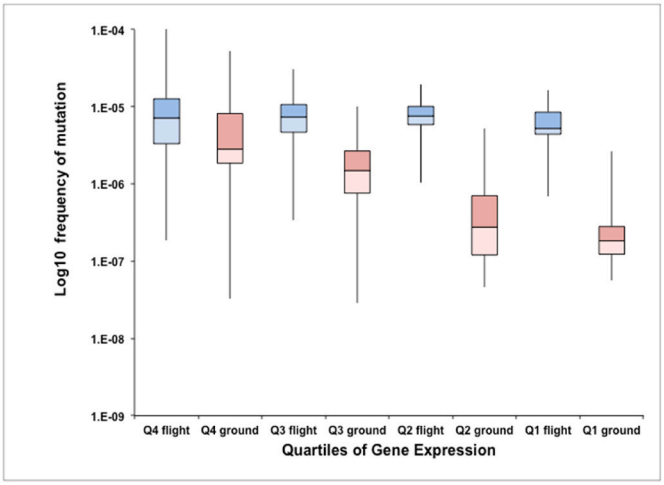

Fig. 5B. Tissue-specific mutation associated with RNA transcription during spaceflight on the ISS relative to ground controls—Skeletal Muscle (quadriceps). Box plot graph of the statistical distribution of exonic mutation frequency (log10 of frequency of mutation) *vs.* significant differential gene expression in different gene expression quartiles for GLDS-103 (quad. muscle) samples on the ISS (blue) relative to ground controls (red). Medians (bar in between dark blue and light blue boxes) for spaceflight gene expression quartiles Q4, Q3, Q2 and Q1 are 7.17e-6, 7.28e-6, 7.52e-6 and 5.22e-6 for number of genes 58, 63, 38 and 13 respectively. Medians for ground control gene expression quartiles Q4, Q3, Q2 and Q1 are 2.82e-6, 1.549e-6, 2.61e-7 and 1.83e-7 for the related number of mutated genes 58, 63, 38 and 13 respectively.

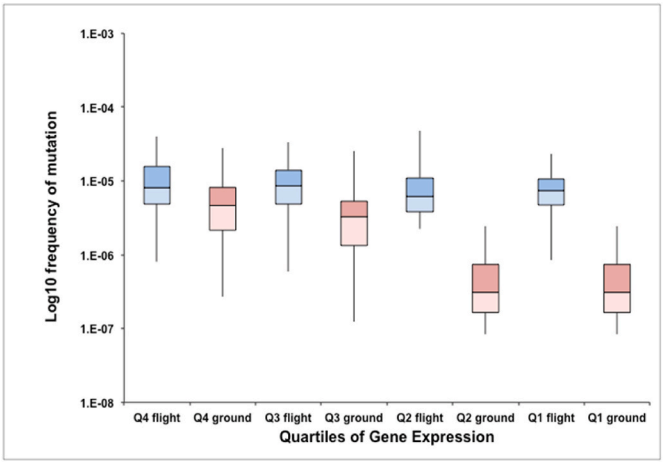

Fig. 5C. Tissue-specific mutation associated with RNA transcription during spaceflight on the ISS relative to ground controls—Liver. Box plot graph of the statistical distribution of exonic mutation frequency (log10 of frequency of mutation) *vs.* significant differential gene expression in different gene expression quartiles for GLDS-137 (liver) samples on the ISS (blue) relative to ground controls (red). Medians for spaceflight gene expression quartiles Q4, Q3, Q2 and Q1 are 8.05e-6, 8.56e-6. 6.14e-6 and 7.39e-6 for number of genes 61, 61, 53 and 71 respectively. Medians for ground control gene expression quartiles Q4, Q3, Q2 and Q1 are 4.66e-6, 3.29e-6, 7.35e-7 and 3.16e-7 for the related number of mutated genes respectively.

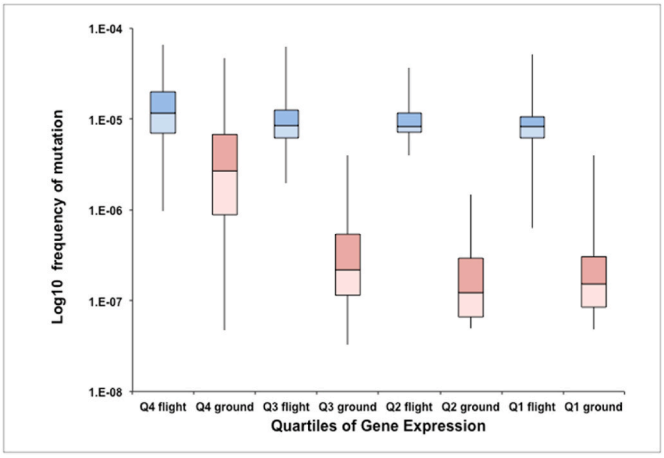

Fig. 5D. Tissue-specific mutation associated with RNA transcription during spaceflight on the ISS relative to ground controls—Eye. Box plot graph of the statistical distribution of exonic mutation frequency (log10 of frequency of mutation) *vs.* significant differential gene expression in different gene expression quartiles for GLDS-162 (eye) samples on the ISS (blue) relative to ground controls (red). Medians (bar in between dark blue and light blue boxes) for spaceflight gene expression quartiles Q4, Q3, Q2 and Q1 1.15e-5, 8.357e-6, 8.37e-6 and 8.24e-6 for number of genes 132, 91, 75 and 66, respectively. Medians for ground control gene expression quartiles Q4, Q3, Q2 and Q1 are 2.69e-6, 2.19e-7, 3.96e-7 and 1.253e-7 for the related number of mutated genes 128, 57, 24 and 14 respectively.

likely decrease tissue functions and cause associated health detriments. Supplementary Table 14 shows SNVs in 249 commonly mutated genes in eye, kidney, quad muscle, and liver tissues that represent hotspots of hypermutation induced on the ISS. These results agree with the previously described RNA–DNA sequence differences (RDDs) in mRNAs, which functionally diversified the proteome beyond DNA encoded functions [44].

Therefore, spaceflight induced NSMs were evaluated for their likely effect on protein function based on sequence homology and on the physical properties of amino acids using the SIFT algorithm [45]. This analysis can distinguish between tolerant and intolerant amino acid substitutions in protein functions. Intriguingly, several spaceflight-induced NSMs can account for some of the common spaceflight-associated risks defined by NASA's Human Research Program (HRP), including muscle atrophy, the SANS, increased risk for kidney stone formation, as well as liver damage and bone density loss [4]. Some genes accumulated several NSMs with intolerant amino acid substitutions, which were mapped in up to 100 % of all tissue samples and encoded functions relevant to the NASA HRP risks (Supplementary Tables 5A–8A). In comparison to the human transcriptome, where peptide sequences that correspond to RNA variant sequences, but not the DNA coding sequences, were found by mass spectrometry, showed that the variants are translated into proteins [46].

The correlation of NSMs to possible causation of health phenotypes on the ISS is additionally corroborated by the evidence of changes in mice stress behavior [47], blood chemistry (e.g., lipidosis, which resulted from direct oxidative damage of lipids) [48], and muscle atrophy [49]. Moreover, hyperactive movements of mice lacking diurnal activity on the ISS in comparison to ground controls also showed evidence of sleeplessness, which is likely due to neurons responsible for arousal that are directly triggered by CO_2 and cause mice to wake up and maintain vigilance on the ISS relative to ground controls [50]. In humans, the retention of CO_2 in the blood is linked with sleep disorders that affect breathing, especially sleep apnea, central hypoventilation syndrome and obesity hypoventilation syndrome [51].

As shown in Supplemental Tables 5–8, NSMs that indicate spaceflight-associated health risks in eye tissue map to known genes, such as *AQP* (encoding the aquaporin pore channel), involved in intraocular pressure regulation by transporting water along an osmotic gradient, which – when defective – can cause an imbalance in the ocular fluid movement and the SANS. Similarly, muscle specific NSMs map to genes that encode the molecular mechanism of muscle contraction, such as *ACTA1* (encoding actin) and *MSTN* and *MYO* (encoding myostatin and myosin), which – when defective – can cause muscle loss and atrophy [52], while kidney specific NSMs map to genes that cause a defect in kidney size and glomerular podocyte morphology, such as *TNS1*, *NPNT* and *CLDN2*, strongly correlated with pathogenic processes in the kidney, including renal stone formation. Also, consistent with the increased liver specific NSMs, such as in *SCP2* and *PLPPR1*, induced in the BALB/c and C57BL/6J mouse strains on the ISS, previous spaceflight studies have found liver damage in both strains of mice within less than 2 weeks aboard the space shuttle and on the ISS [53]. The spaceflight induced liver damage included defects in several affected gene expression pathways that resulted in altered lipid metabolism, fatty acid metabolism, lipid and fatty acid processing, lipid catabolic processing, and lipid localization [52]. Remarkably, liver damage affecting the retinol biosynthesis can also lead to bone demineralization and fractures in animals and in humans [54], while long-term treatment with synthetic retinoids has been linked with decreased bone density and osteoporosis [48]. Consistently, some of the genes that control the availability of retinol in liver [52] were also identified to have multiple NSMs induced in mice on the ISS relative to ground controls (Supplementary Tables 5A–8A).

Also, SNVs were mapped to the ribosomal RNA gene, *Rn45s* (Supplementary Table 15). For example, eye tissue from the ISS had about 2 times more unique SNVs (on average per sample) than in liver tissue, and about 3 times more unique SNVs (on average per sample) than in the muscle tissue relative to ground controls. This additionally confirms tissue-specific, varied mutation rates catalyzed by unique metabolic processes and varied effects of the increased partial pressure of CO_2 on the ISS.

Functional and pathway analysis of the ISS mutated genes relative to ground controls in eye tissue identified enriched cellular processes that are consistent with a growing number of studies that implicate endoplasmic reticulum (ER) stress in the trabecular meshwork of the eye as a

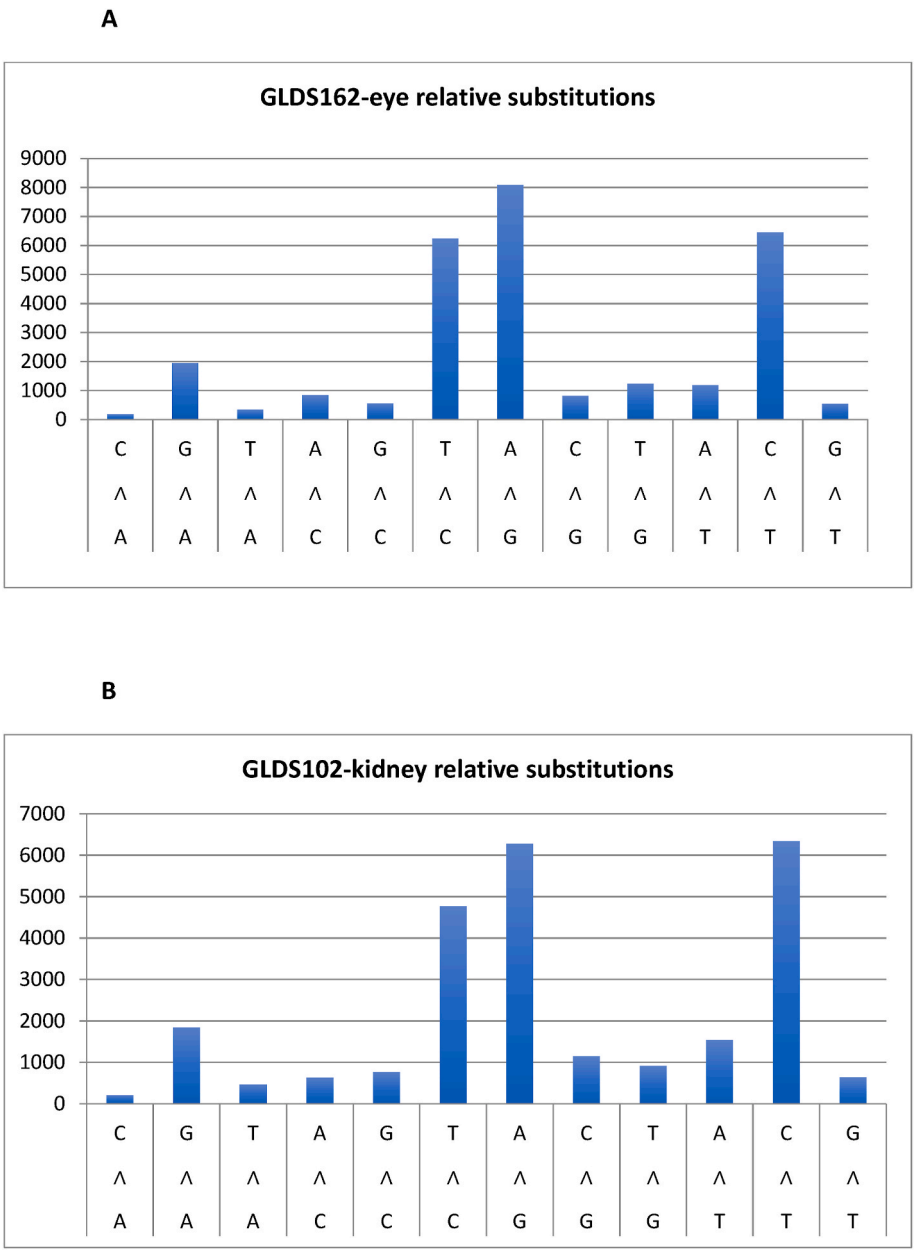

Fig. 6A–D. The relative proportion of each type of base substitution in SNVs (somatic mutations) in mRNAs induced on the ISS relative to ground controls is similar in each tissue - GLDS162-eye (A), GLDS102-kidney (B), GLDS137-liver (C) and GLDS103-skeletal muscle (quadriceps) (D). Guanine base substitutions were the most common. By comparison, RNA editing-type base substitutions (in humans) are known to involve primarily adenine substitution.

cause for increase in IOP, and found corresponding genes involved in reduction of ER stress that can prevent ocular pathologies in glaucoma mouse models as well as in lipid biosynthesis. Lipids are energy substrates for mitochondria in photoreceptors and eye dyslipidemia is characterized by an abnormal circulating lipid profile including triglycerides, cholesterol, low-density lipoproteins, high-density lipoproteins, or polyunsaturated fatty acids, which contribute to the development and progression of retinal dysfunction in many eye diseases and age-related macular degeneration. Also, the biological meaning of the ISS mutated genes that encode structural constituents of eye lens was identified as significantly enriched using the DAVID algorithm. Similarly, functional and pathway analysis of the ISS mutated genes in kidney, quad muscle, and liver tissues identified their corresponding tissue specific enriched cellular processes (Supplementary Tables 10–12).

Additionally, up to 4.2 % of SNVs induced by ISS relative to ground controls in the BALB/c and C57BL/6J mouse strains, depending on the tissue type, were found at identical genome-wide coordinates in other mouse strains that never flew in space (Supplementary Table 13). This concordance was observed in the mouse dbSNP, *i.e.*, in the dbSNP142 version, which is a high-quality single nucleotide polymorphism (SNP) database with more than 80 million SNVs mapped in DNA from 36 inbred strains of laboratory mice, drawn from several sources [55]. The improbability of mutating the BALB/c or C57BL/6J strains on the ISS at some of the same genome-wide coordinates as found in other inbred mouse strains that never flew in space is extremely small, suggesting hotspots of sequence variation in the mouse genome. These results are like the identical RDD sites in yeast mRNAs, which functionally diversified the proteome beyond DNA encoded functions in several wild-type yeast strain [44].

C

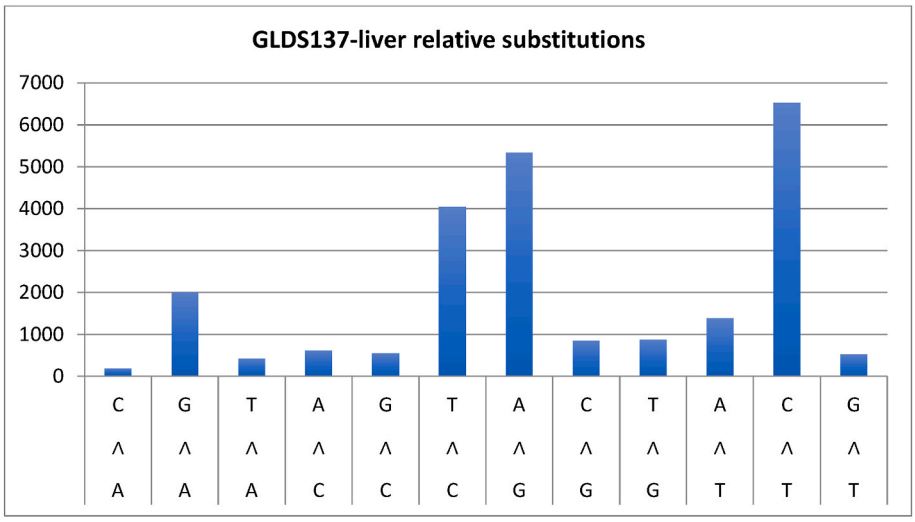

D

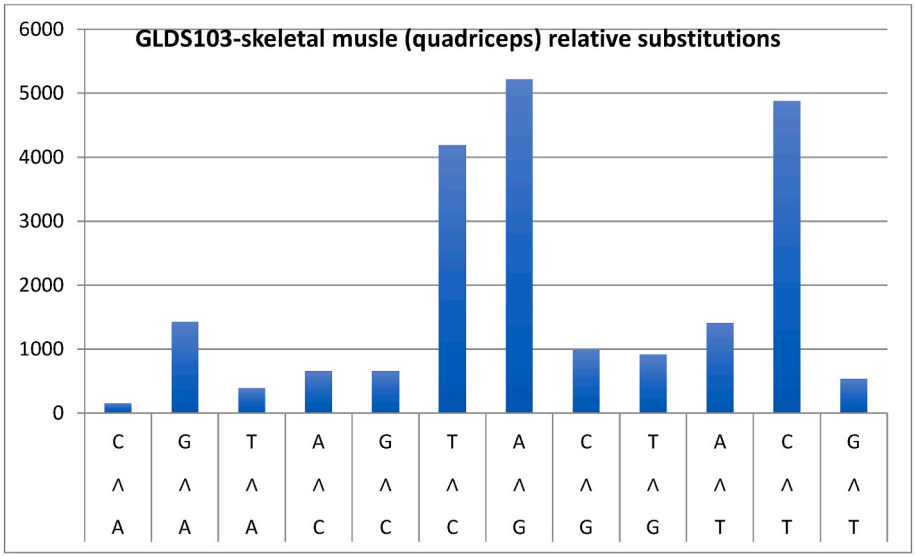

Fig. 6A–D. (*continued*).

Interestingly, most mutations induced on the ISS mapped to the mice coding-rather than non-coding sequences (Supplementary Table 17). This coding specificity of the ISS induced mutations is in contrast with the results of the Catalogue Of Somatic Mutations In Cancer v86, which mapped most mutations (77 %) in the non-coding sequences [56]. This incongruent result suggests that altered chromatin in spaceflight fails to protect the exome against mutation by losing its known highest protective coverage of nucleosomes in the exons [57]. Therefore, on the ISS relative to ground controls, the dynamic re-positioning of nucleosomes during transcription likely fails to protect the exome from mutation induced by metabolically generated ROS. This view of altered chromatin exposing genes to ROS is also consistent with studies that identified strand specific accumulation of mutations in actively transcribed yeast and human genes, where hypermutation *via* multiple simultaneous changes in ssDNA along the same strand has been identified [58,59].

4. Discussion

Our study of somatic mutation in mice flown to the ISS is the first comprehensive assessment of somatic mutation accumulation in any mammalian system in space. Our study takes advantage of the availability of gene expression data in mice obtained as part of four validation studies, conducted several years ago, that were some of the first investigations to employ next generation sequencing on mammalian tissue specimens from space. Unexpectedly, we identified a high rate of genome-wide somatic mutation (single nucleotide variants) in the experimental animals flown on the ISS. It should be emphasized that physiological endpoints, or endpoints related to the development of malignancies, were not part of the study design. Therefore, the consequences of these somatic mutations cannot be addressed. Nonetheless, the tissue specificity of the mutations and their mapping to mammalian genes with spaceflight relevant function suggests that induction of somatic mutation in space may contribute to spaceflight pathophysiology, although a human study of somatic mutation during spaceflight has not

yet been carried out. Our results are specifically relevant to spaceflight aboard the ISS, an environment with elevated carbon dioxide levels. Within the ISS, which is located in a Low Earth Orbit, ionizing radiation is also increased, as a result of decreased shielding by the Earth's magnetosphere. Daily ionization radiation exposure (effective dose) on the ISS is approximately 0.5 mSv per day, compared to 0.006 mSv on Earth [60].

The phenomenon of somatic mutation has been appreciated for decades, primarily in cancer cells. In the last 15 years, with the advent of next generation sequencing, it has become much easier to examine somatic mutation quantitatively, and to look at somatic mutation in normal cells and tissues, not just in malignant cells. It is now well understood that somatic mutations accumulate gradually over time, in all tissues. For reasons that are not entirely clear, the rate of somatic mutation accumulation varies more than 10-fold across the full range of tissue types [61,62].

Various exogenous factors can lead to an increase in the rate of somatic mutation accumulation in mammalian tissue, and it is worthwhile to briefly review this topic. Broadly speaking, ionizing radiation, exposure to certain chemical compounds, and intracellular processes generating free radicals are stressors placed on the cell that can cause mutations within DNA [63]. Mice irradiated with X-rays, for example, show a modest increase in single nucleotide variants (27 %) per 1 Gy of radiation, in hematopoietic stem cells [64]. Certain chemotherapy agents are among the most powerful inducers of somatic mutation. While chemotherapy-induced somatic mutation can be seen in cancer cells themselves (resulting in the acquisition of mutations that lead to resistance to chemotherapy), somatic mutation is also observed in normal tissues in patients who are undergoing chemotherapy [65]. Platinum-containing chemotherapy agents are the most potent inducers of somatic mutation, capable of increasing the rate of somatic mutation more than 100-fold. The effect seems to be strongly correlated with guanine oxidation [66]. Unsurprisingly, in mutant *Drosophila melanogaster* that are oxidant sensitive (urate-null *Drosophila*), both chemical clastogens and radiation (X-rays) cause somatic mutation at rates higher than in wild-type *Drosophila*. This result suggests that common final pathways involving oxidative stress are involved in both radiation and chemical-induced somatic mutation [67].

Because the mice in our study were exposed to only modestly elevated levels of ionizing radiation—not enough to account for the greatly increased rate of somatic mutation accumulation we observed—we considered the possibility that significantly elevated levels of carbon dioxide on board the ISS may have contributed to the development somatic mutations. On the ISS, carbon dioxide levels are increased significantly. Expressed as partial pressures, CO_2 levels are approximately 3.41 ± 0.93 mmHg on the ISS [68], compared to terrestrial levels of approximately 0.32 mm Hg. It is well known that in cells, CO_2 is an important byproduct of metabolism. Carbon dioxide, in equilibrium with bicarbonate anion (HCO_3^-) in aqueous environments, is also an important pH buffer. Less well known, however, is the fact that CO_2 plays an important role in reactive oxygen species (ROS) reactions with macromolecules. The main ROS, superoxide anion ($O_2^{\bullet-}$), hydrogen peroxide (H_2O_2) and the hydroxyl radical ($HO^\bullet$), can all oxidize biological macromolecules, such as proteins, amino acids, cell membranes and nucleic acids. Some of these reactions, however, are dependent on the presence of bicarbonate anion (HCO_3^-) [69–71]. In a recent study, Ezraty and co-workers demonstrated that CO_2 increases $HO^\bullet$ toxicity and increases H_2O_2-dependent mutation frequency in *E. coli* [72]. CO_2 also increases H_2O_2-dependent 8-oxo-guanine DNA damage. The mechanism may involve the formation of the carbonate radical anion ($CO_3^{\bullet-}$) from bicarbonate anion and hydroxyl radicals [73], since carbonate radical is a strong oxidant that can oxidize guanine [74,75]. The formation of peroxymonocarbonate (HCO_4^-) may also be involved, as peroxymonocarbonate can be formed from bicarbonate and hydrogen peroxide [76]. Peroxymonocarbonate is another strong oxidant that can react with a variety of organic compounds [77].

The DNA base substitution pattern that we determined from analysis of the RNA-Seq data allows us to make several important conclusions, although, ultimately, the story is incomplete. First and foremost, we did not see a strong pattern of adenine substitution (A > C or A > T transversions, or A > G transition). A predominance of adenine substitution, inferred from RNA-Seq data, would have suggested that we were looking at RNA editing *via* adenosine deaminase, not direct changes in the DNA sequence [78]. That pattern was not seen. Instead, we saw a predominance of G > A transitions and C > T transitions. These observations are consistent with oxidative mutagenesis involving guanine oxidation and oxidative deamination of cytosine. In addition to G > A and C > T transitions, T > C transitions were also seen in high numbers. An explanation for the T > C transitions, however, is not readily available. Transversions (purine to pyrimidine substitutions, and pyrimidine to purine substitutions) happened much less frequently.

In summary, this is the first documented experimental evidence for increased somatic mutation in a mammalian species in the space environment, although several ground-based experimental systems have hinted at this possibility [79]. Importantly, none of the ground-based analog investigations probing the topic of genome instability, thus far, have included elevated carbon dioxide levels as part of the experimental conditions. Since the levels of ionizing radiation aboard the ISS are only slightly elevated versus conditions on Earth, we favor an explanation for the accelerated mutation on the ISS based on oxidant reactions involving elevated CO_2 levels. Our analysis of the spectrum of base substitutions, which shows a predominance of guanine transitions and cytosine transitions, is consistent with this explanation, although we acknowledge that the exact molecular mechanisms cannot yet be determined. We acknowledge that physiological effects related to weightlessness may contribute to the oxidant environment that leads to somatic mutation. While the significance of these somatic mutations cannot be gauged at this time, our findings in mice provide compelling motivation for a study of somatic mutation in astronauts in the space environment.

CRediT authorship contribution statement

Viktor Stolc: Conceptualization, Data curation, Formal analysis, Funding acquisition, Investigation, Methodology, Project administration, Resources, Software, Supervision, Validation, Visualization, Writing – original draft, Writing – review & editing. **Miloslav Karhanek:** Conceptualization, Data curation, Formal analysis, Investigation, Methodology, Resources, Software, Validation, Visualization, Writing – original draft, Writing – review & editing. **Friedemann Freund:** Investigation, Methodology, Visualization, Writing – original draft, Writing – review & editing. **Yuri Griko:** Conceptualization, Investigation, Methodology, Writing – review & editing. **David J. Loftus:** Formal analysis, Funding acquisition, Investigation, Validation, Writing – original draft, Writing – review & editing. **Maurice M. Ohayon:** Conceptualization, Investigation, Methodology, Validation, Writing – original draft, Writing – review & editing.

Data availability

RNA-seq data generated in this study are deposited to the NASA GeneLab database [https://genelab.nasa.gov/]. All analyses were conducted using standard software. The settings of software used for analyses are described in the Methods. Source data are provided with this paper. The data underlying this article are available in the article and in its online supplementary material.

Source data

GLDS-102**:** Rodent Research-1 (RR1) NASA Validation Flight: Mouse kidney transcriptomic, proteomic, and epigenomic data.

GLDS-103**:** Rodent Research-1 (RR1) NASA Validation Flight: Mouse quadriceps muscle transcriptomic, proteomic, and epigenomic data.

GLDS-137: Rodent Research-3-CASIS: Mouse liver transcriptomic, proteomic, and epigenomic data.

GLDS-162: Rodent Research-3-CASIS: Mouse eye transcriptomic and proteomic data.

Permissions

Not applicable.

Funding

This research was supported by NASA ITA#16274 and the NASA Human Research Program to V.S.

Declaration of competing interest

None.

Acknowledgements

We thank the NASA Human Research Program for making this work possible.

Appendix A. Supplementary data

Supplementary data to this article can be found online at https://doi.org/10.1016/j.redox.2024.103398.

References

[1] E. Uffelmann, Q.Q. Huang, N.S. Munung, Jantina de Vries, Y. Okada, A.R. Martin, H.C. Martin, T. Lappalainen, D. Posthuma, Genome-wide association studies, Nat Rev Methods Primers 1 (2021) 59, https://doi.org/10.1038/s43586-021-00056-9.

[2] Committee to Review NASA's Evidence Reports on Human Health Risks, Board on Health Sciences Policy, Health and Medicine Division, & National Academies of Sciences, Engineering, and Medicine. Review of NASA's Evidence Reports on Human Health Risks: 2017 Letter Report. 24953, National Academies Press, 2018, https://doi.org/10.17226/24953.

[3] I. Martincorena, P.J. Campbell, Somatic mutation in cancer and normal cells, Science (New York, N.Y.) 349 (2015) 1483–1489, https://doi.org/10.1126/science.aab4082.

[4] NASA, Human research program integrated research plan. https://humanresearchroadmap.nasa.gov.

[5] A. Beheshti, J. Miller, Y. Kidane, D. Berrios, S.G. Gebre, S.V. Costes, NASA GeneLab Project: bridging space radiation omics with ground studies, Radiat. Res. 189 (1) (2018) 553–559, https://doi.org/10.1667/RR15062.

[6] J.F. Sollner, G. Leparc, T. Hildebrandt, H. Klein, L. Thomas, E. Stupka, E. Simon, An RNA-Seq atlas of gene expression in mouse and rat normal tissues, Sci. Data 4 (2017) 170185, https://doi.org/10.1038/sdata.2017.185.

[7] P. Krusche, L. Trigg, P.C. Boutros, C.E. Mason, F.M. De La Vega, B.L. Moore, M. Gonzalez-Porta, M.A. Eberle, Z. Tezak, S. Lababidi, et al., Best practices for benchmarking germline small-variant calls in human genomes, Nat. Biotechnol. 37 (2019) 555–560, https://doi.org/10.1038/s41587-019-0054-x.

[8] K. Cibulskis, M.S. Lawrence, S.L. Carter, A. Sivachenko, D. Jaffe, C. Sougnez, S. Gabriel, M. Meyerson, E.S. Lander, G. Getz, Sensitive detection of somatic point mutations in impure and heterogeneous cancer samples, Nat. Biotechnol. 31 (2013) 213–219, https://doi.org/10.1038/nbt.2514.

[9] J.M. Zook, J. McDaniel, N.D. Olson, J. Wagner, H. Parikh, H. Heaton, S.A. Irvine, L. Trigg, R. Truty, C.Y. McLean, F.M. De La Vega, C. Xiao, S. Sherry, M. Salit, An open resource for accurately benchmarking small variant and reference calls, Nat. Biotechnol. 37 (2019) 561–566, https://doi.org/10.1038/s41587-019-0074-6.

[10] K. Wang, M. Li, H. Hakonarson, ANNOVAR: functional annotation of genetic variants from high-throughput sequencing data, Nucleic Acids Res. 38 (2010) e164, https://doi.org/10.1093/nar/gkq603.

[11] W. McLaren, L. Gil, S.E. Hunt, H.S. Riat, G.R. Ritchie, A. Thormann, P. Flicek, F. Cunningham, The Ensembl variant effect predictor, Genome Biol. 17 (2016) 122, https://doi.org/10.1186/s13059-016-0974-4.

[12] N.L. Bray, H. Pimentel, P. Melsted, L. Pachter, Near-optimal probabilistic RNA-seq quantification, Nat. Biotechnol. 34 (2016) 525–527, https://doi.org/10.1038/nbt.3519.

[13] G.P. Wagner, K. Kin, V.J. Lynch, Measurement of mRNA abundance using RNA-seq data: RPKM measure is inconsistent among samples, Theory in biosciences =Theorie in den Biowissenschaften 131 (2012) 281–285, https://doi.org/10.1007/s12064-012-0162-3.

[14] S.J. Balin, M. Cascalho, The rate of mutation of a single gene, Nucleic Acids Res. 38 (2010) 1575–1582, https://doi.org/10.1093/nar/gkp1119.

[15] A. Coudray, A.M. Battenhouse, P. Bucher, V.R. Iyer, Detection and benchmarking of somatic mutations in cancer genomes using RNA-seq data, PeerJ 6 (2018) e5362, https://doi.org/10.7717/peerj.5362.

[16] I.F. do Valle, E. Giampieri, G. Simonetti, A. Padella, M. Manfrini, A. Ferrari, C. Papayannidis, I. Zironi, M. Garonzi, S. Bernardi, et al., Optimized pipeline of MuTect and GATK tools to improve the detection of somatic single nucleotide polymorphisms in whole-exome sequencing data, BMC Bioinf. 17 (2016) 341, https://doi.org/10.1186/s12859-016-1190-7.

[17] A. Kumar, S. Adhikari, M. Kankainen, C.A. Heckman, Comparison of structural and short variants detected by linked-read and whole-exome sequencing in multiple myeloma, Cancers 13 (2021) 1212, https://doi.org/10.3390/cancers13061212.

[18] V.K. Sarsani, N. Raghupathy, I.T. Fiddes, J. Armstrong, F. Thibaud-Nissen, O. Zinder, M. Bolisetty, K. Howe, D. Hinerfeld, X. Ruan, et al., The genome of C57BL/6J "Eve", the mother of the laboratory mouse genome reference strain, G3 (Bethesda, Md.) 9 (2019) 1795–1805, https://doi.org/10.1016/j.xgen.2023.100291.

[19] A.B. Adewoye, S.J. Lindsay, Y.E. Dubrova, M.E. Hurles, The genome-wide effects of ionizing radiation on mutation induction in the mammalian germline, Nat. Commun. 6 (2015) 6684, https://doi.org/10.1038/ncomms7684.

[20] P.E. García-Nieto, A.J. Morrison, H.B. Fraser, The somatic mutation landscape of the human body, Genome Biol. 20 (2019) 298, https://doi.org/10.1186/s13059-019-1919-5.

[21] Y. Oji, N. Tatsumi, M. Fukuda, S. Nakatsuka, S. Aoyagi, E. Hirata, I. Nanchi, F. Fujiki, H. Nakajima, Y. Yamamoto, et al., The translation elongation factor eEF2 is a novel tumor-associated antigen overexpressed in various types of cancers, Int. J. Oncol. 44 (2014) 1461–1469, https://doi.org/10.3892/ijo.2014.2318.

[22] C.M. Wong, K.L. Siu, D.Y. Jin, Peroxiredoxin-null yeast cells are hypersensitive to oxidative stress and are genomically unstable, J. Biol. Chem. 279 (2004) 23207–23213, https://doi.org/10.1074/jbc.M402095200.

[23] P. Potluri, A. Davila, E. Ruiz-Pesini, D. Mishmar, S. O'Hearn, S. Hancock, M. Simon, I.E. Scheffler, D.C. Wallace, V. Procaccio, A novel NDUFA1 mutation leads to a progressive mitochondrial complex I-specific neurodegenerative disease, Mol. Genet. Metabol. 96 (2009) 189–195, https://doi.org/10.1016/j.ymgme.2008.12.004.

[24] S. Obeid, N. Blatter, R. Kranaster, A. Schnur, K. Diederichs, W. Welte, A. Marx, Replication through an abasic DNA lesion: structural basis for adenine selectivity, EMBO J. 29 (2010) 1738–1747, https://doi.org/10.1038/emboj.2010.64.

[25] M.F. Montiel-Gonzalez, F.J. Diaz Quiroz, J.J.C. Rosenthal, Current strategies for site-directed RNA editing using ADARs, Methods 156 (2019) 16–24, https://doi.org/10.1016/j.ymeth.2018.11.016.

[26] A.M. Fleming, Y. Ding, C.J. Burrows, Sequencing DNA for the oxidatively modified base 8-oxo-7,8-dihydroguanine, Methods Enzymol. 591 (2017) 187–210, https://doi.org/10.1016/bs.mie.2017.03.004.

[27] K. Kino, M. Hirao-Suzuki, M. Morikawa, A. Sakaga, H. Miyazawa, Generation, repair and replication of guanine oxidation products, Gene Environ.: the official journal of the Japanese Environmental Mutagen Society 39 (2017) 21, https://doi.org/10.1186/s41021-017-0081-0.

[28] D.A. Kreutzer, J.M. Essigmann, Oxidized, deaminated cytosines are a source of C–>T transitions in vivo, Proc. Natl. Acad. Sci. U.S.A. 95 (1998) 3578–3582, https://doi.org/10.1073/pnas.95.7.3578.

[29] V. Stolc, A. Shmygelska, Y. Griko, Adaptation of organisms by resonance of RNA transcription with the cellular redox cycle, PLoS One 6 (2011) e25270, https://doi.org/10.1371/journal.pone.0025270.

[30] H. Liu, Q. Wang, Y. He, L. Chen, C. Hao, C. Jiang, Y. Li, Y. Dai, Z. Kang, J.R. Xu, Genome-wide A-to-I RNA editing in fungi independent of ADAR enzymes, Genome Res. 26 (2016) 499–509, https://doi.org/10.1101/gr.199877.115.

[31] B.L. Bass, RNA editing by adenosine deaminases that act on RNA, Annu. Rev. Biochem. 71 (2002) 817–846, https://doi.org/10.1146/annurev.biochem.71.110601.135501.

[32] V. D'Annibale, A.N. Nardi, A. Amadei, M. D'Abramo, Theoretical characterization of the reduction potentials of nucleic acids in solution, J. Chem. Theor. Comput. 17 (2021) 1301–1307, https://doi.org/10.1021/acs.jctc.0c00728.

[33] Z. Fu, C.T. Chen, G. Cagnone, E. Heckel, Y. Sun, B. Cakir, Y. Tomita, S. Huang, Q. Li, W. Britton, et al., Dyslipidemia in retinal metabolic disorders, EMBO Mol. Med. 11 (2019) e10473, https://doi.org/10.15252/emmm.201910473.

[34] J.T. Eells, Mitochondrial dysfunction in the aging retina, Biology 8 (2019) 31, https://doi.org/10.3390/biology8020031.

[35] G. Trudel, N. Shahin, T. Ramsay, O. Laneuville, H. Louati, Hemolysis contributes to anemia during long-duration space flight, Nat. Med. 28 (2022) 59–62, https://doi.org/10.1038/s41591-021-01637-7.

[36] V. Bhandari, C. Hoey, L.Y. Liu, E. Lalonde, J. Ray, J. Livingstone, R. Lesurf, Y. J. Shiah, T. Vujcic, Huang, et al., Molecular landmarks of tumor hypoxia across cancer types, Nat. Genet. 51 (2019) 308–318, https://doi.org/10.1038/s41588-018-0318-2.

[37] V. Bhandari, C.H. Li, R.G. Bristow, P.C. Boutros, P.C.A.W.G. Consortium, Divergent mutational processes distinguish hypoxic and normoxic tumours, Nat. Commun. 11 (2020) 737, https://doi.org/10.1038/s41467-019-14052-x.

[38] R.G. Bristow, R.P. Hill, Hypoxia and metabolism. Hypoxia, DNA repair and genetic instability, Nat. Rev. Cancer 8 (2008) 180–192, https://doi.org/10.1038/nrc2344.

[39] Y. Benita, H. Kikuchi, A.D. Smith, M.Q. Zhang, D.C. Chung, R.J. Xavier, An integrative genomics approach identifies Hypoxia Inducible Factor-1 (HIF-1)-target genes that form the core response to hypoxia, Nucleic Acids Res. 37 (2009) 4587–4602, https://doi.org/10.1093/nar/gkp425.

[40] L.E. Huang, J. Gu, M. Schau, H.F. Bunn, Regulation of hypoxia-inducible factor 1alpha is mediated by an O2-dependent degradation domain via the ubiquitin-proteasome pathway, Proc. Natl. Acad. Sci. U.S.A. 95 (1998) 7987–7992, https://doi.org/10.1073/pnas.95.14.7987.

[41] Y.A. Pérez-Rico, V. Boeva, A.C. Mallory, A. Bitetti, S. Majello, E. Barillot, A. Shkumatava, Comparative analyses of super-enhancers reveal conserved elements in vertebrate genomes, Genome Res. 27 (2017) 259–268, https://doi.org/10.1101/gr.203679.115.
[42] N.S. Wickramasinghe, T.T. Manavalan, S.M. Dougherty, K.A. Riggs, Y. Li, C. M. Klinge, Estradiol downregulates miR-21 expression and increases miR-21 target gene expression in MCF-7 breast cancer cells, Nucleic Acids Res. 37 (2009) 2584–2595, https://doi.org/10.1093/nar/gkp117.
[43] F. Meng, R. Henson, H. Wehbe-Janek, K. Ghoshal, S.T. Jacob, T. Patel, MicroRNA-21 regulates expression of the PTEN tumor suppressor gene in human hepatocellular cancer, Gastroenterology 133 (2007) 647–658, https://doi.org/10.1053/j.gastro.2007.05.022.
[44] I.X. Wang, C. Grunseich, Y.G. Chung, H. Kwak, G. Ramrattan, Z. Zhu, V.G. Cheung, RNA-DNA sequence differences in, Saccharomyces cerevisiae, Genome Res. 26 (2016) 1544–1554, https://doi.org/10.1101/gr.207878.116.
[45] P. Kumar, S. Henikoff, P.C. Ng, Predicting the effects of coding non-synonymous variants on protein function using the SIFT algorithm, Nat. Protoc. 4 (2009) 1073–1081, https://doi.org/10.1038/nprot.2009.86.
[46] M. Li, I.X. Wang, Y. Li, A. Bruzel, A.L. Richards, J.M. Toung, V.G. Cheung, Widespread RNA and DNA sequence differences in the human transcriptome, Science 333 (2011) 53–58, https://doi.org/10.1126/science.1207018.
[47] S.Y. Choi, A. Saravia-Butler, Y. Shirazi-Fard, D. Leveson-Gower, L.S. Stodieck, S. M. Cadena, J. Beegle, S. Solis, A. Ronca, R.K. Globus, Validation of a new rodent experimental system to investigate consequences of long duration space habitation, Sci. Rep. 10 (2020) 2336, https://doi.org/10.1038/s41598-020-58898-4.
[48] A.C. Ross, R. Zolfaghari, Regulation of hepatic retinol metabolism: perspectives from studies on vitamin A status, J. Nutr. 134 (2004) 269S–275S, https://doi.org/10.1093/jn/134.1.269S.
[49] S.J. Lee, A. Lehar, J.U. Meir, C. Koch, A. Morgan, L.E. Warren, R. Rydzik, D. W. Youngstrom, H. Chandok, J. George, et al., Targeting myostatin/activin A protects against skeletal muscle and bone loss during spaceflight, Proc. Natl. Acad. Sci. U.S.A. 117 (2020) 23942–23951, https://doi.org/10.1073/pnas.2014716117.
[50] H.R. Smith, N.K. Leibold, D.A. Rappoport, C.M. Ginapp, B.S. Purnell, N.M. Bode, S. L. Alberico, Y.C. Kim, E. Audero, C.T. Gross, G.F. Buchanan, Dorsal raphe serotonin neurons mediate CO2-induced arousal from sleep, J. Neurosci.: the official journal of the Society for Neuroscience 38 (2018) 1915–1925, https://doi.org/10.1523/JNEUROSCI.2182-17.2018.
[51] J.F. Masa, J.L. Pépin, J.C. Borel, B. Mokhlesi, P.B. Murphy, M.A. Sánchez-Quiroga, Obesity hypoventilation syndrome, Eur. Respir. Rev. : an official journal of the European Respiratory Society 28 (2019) 180097, https://doi.org/10.1183/16000617.0097-2018.
[52] A. Beheshti, K. Chakravarty, H. Fogle, H. Fazelinia, W.A.D. Silveira, V. Boyko, S. L. Polo, A.M. Saravia-Butler, G. Hardiman, D. Taylor, et al., Multi-omics analysis of multiple missions to space reveal a theme of lipid dysregulation in mouse liver, Sci. Rep. 9 (2019) 19195, https://doi.org/10.1038/s41598-019-55869-2.
[53] K.R. Jonscher, A. Alfonso-Garcia, J.L. Suhalim, D.J. Orlicky, E.O. Potma, V. L. Ferguson, M.L. Bouxsein, T.A. Bateman, L.S. Stodieck, M. Levi, et al., Spaceflight activates lipotoxic pathways in mouse liver, PLoS One 11 (2016) e0152877, https://doi.org/10.1371/journal.pone.0152877.
[54] J.H. Promislow, D. Goodman-Gruen, D.J. Slymen, E. Barrett-Connor, Retinol intake and bone mineral density in the elderly: the Rancho Bernardo Study, J. Bone Miner. Res.: the official journal of the American Society for Bone and Mineral Research 17 (2002) 1349–1358, https://doi.org/10.1359/jbmr.2002.17.8.1349.
[55] MGI. Search Mouse SNPs (https://www.informatics.jax.org).
[56] J.G. Tate, S. Bamford, H.C. Jubb, Z. Sondka, D.M. Beare, N. Bindal, H. Boutselakis, C.G. Cole, C. Creatore, E. Dawson, et al., COSMIC: the Catalogue of somatic mutations, Cancer. Nucleic acids research 47 (2019) D941–D947, https://doi.org/10.1093/nar/gky1015.
[57] H. Tilgner, C. Nikolaou, S. Althammer, M. Sammeth, M. Beato, J. Valcárcel, R. Guigó, Nucleosome positioning as a determinant of exon recognition, Nat. Struct. Mol. Biol. 16 (2009) 996–1001, https://doi.org/10.1038/nsmb.1658.
[58] S.A. Roberts, J. Sterling, C. Thompson, S. Harris, D. Mav, R. Shah, L.J. Klimczak, G. V. Kryukov, E. Malc, P.A. Mieczkowski, et al., Clustered mutations in yeast and in human cancers can arise from damaged long single-strand DNA regions, Mol. Cell 46 (2012) 424–435, https://doi.org/10.1016/j.molcel.2012.03.030.
[59] K. Chan, D.A. Gordenin, Clusters of multiple mutations: incidence and molecular mechanisms, Annu. Rev. Genet. 49 (2015) 243–267, https://doi.org/10.1146/annurev-genet-112414-054714.
[60] R. Thirsk, A. Kuipers, C. Mukai, D. Williams, The space-flight environment: the international space station and beyond, CMAJ (Can. Med. Assoc. J.) : Canadian Medical Association journal =journal de l'Association medicale canadienne 180 (2009) 1216–1220, https://doi.org/10.1503/cmaj.081125.
[61] D. Hao, L. Wang, Lj Di, Distinct mutation accumulation rates among tissues determine the variation in cancer risk, Sci. Rep. 6 (2016) 19458, https://doi.org/10.1038/srep19458.
[62] B. Milholland, X. Dong, L. Zhang, X. Hao, Y. Suh, J. Vijg, Differences between germline and somatic mutation rates in humans and mice, Nat. Commun. 8 (2017) 15183, https://doi.org/10.1038/ncomms15183.
[63] A. Balmain, The critical roles of somatic mutations and environmental tumor-promoting agents in cancer risk, Nat. Genet. 52 (2020) 1139–1143, https://doi.org/10.1038/s41588-020-00727-5.
[64] Y. Matsuda, A. Uchimura, Y. Satoh, N. Kato, M. Toshishige, J. Kajimura, K. Hamasaki, K. Yoshida, T. Hayashi, A. Noda, O. Tanabe, Spectra and characteristics of somatic mutations induced by ionizing radiation in hematopoietic stem cells, Proc. Natl. Acad. Sci. U.S.A. 120 (2023) e2216550120, https://doi.org/10.1073/pnas.2216550120.
[65] E. Kuijk, O. Kranenburg, E. Cuppen, A. Van Hoeck, Common anti-cancer therapies induce somatic mutations in stem cells of healthy tissue, Nat. Commun. 13 (2022) 5915, https://doi.org/10.1038/s41467-022-33663-5.
[66] S. Afzal, S.A. Jensen, J.B. Sørensen, T. Henriksen, A. Weimann, H.E. Poulsen, Oxidative damage to guanine nucleosides following combination chemotherapy with 5-fluorouracil and oxaliplatin, Cancer Chemother. Pharmacol. 69 (2012) 301–307, https://doi.org/10.1007/s00280-011-1700-2.
[67] R. Koike, T. Uchiyama, S. Arimoto-Kobayashi, K. Okamoto, T. Negishi, Increase of somatic cell mutations in oxidative damage-sensitive drosophila, Gene Environ.: the official journal of the Japanese Environmental Mutagen Society 40 (2018) 3, https://doi.org/10.1186/s41021-017-0090-z.
[68] J. Law, M. Van Baalen, M. Foy, S.S. Mason, C. Mendez, M.L. Wear, V.E. Meyers, D. Alexander, Relationship between carbon dioxide levels and reported headaches on the international space station, J. Occup. Environ. Med. 56 (2014) 477–483, https://doi.org/10.1097/JOM.0000000000000158.
[69] B.S. Berlett, P.B. Chock, M.B. Yim, E.R. Stadtman, Manganese(II) catalyzes the bicarbonate-dependent oxidation of amino acids by hydrogen peroxide and the amino acid-facilitated dismutation of hydrogen peroxide, Proc. Natl. Acad. Sci. U.S. A. 87 (1990) 389–393, https://doi.org/10.1073/pnas.87.1.389.
[70] E.R. Stadtman, B. S Berlett, Fenton chemistry. Amino acid oxidation, J. Biol. Chem. 266 (1991) 17201–17211, https://doi.org/10.1016/S0021-9258(19)47359-6.
[71] S.J. Hug, O. Leupin, Iron-catalyzed oxidation of arsenic(III) by oxygen and by hydrogen peroxide: pH-dependent formation of oxidants in the Fenton reaction, Environ. Sci. Technol. 37 (2003) 2734–2742, https://doi.org/10.1021/es026208x.
[72] B. Ezraty, M. Chabalier, A. Ducret, E. Maisonneuve, S. Dukan, CO2 exacerbates oxygen toxicity, EMBO Rep. 12 (2011) 321–326, https://doi.org/10.1038/embor.2011.7.
[73] S. Yan, Y. Liu, L. Lian, R. Li, J. Ma, H. Zhou, W. Song, Photochemical formation of carbonate radical and its reaction with dissolved organic matters, Water Res. 161 (2019) 288–296, https://doi.org/10.1016/j.watres.2019.06.002.
[74] Y.A. Lee, B.H. Yun, S.K. Kim, Y. Margolin, P.C. Dedon, N.E. Geacintov, V. Shafirovich, Mechanisms of oxidation of guanine in DNA by carbonate radical anion, a decomposition product of nitrosoperoxycarbonate, Chemistry 13 (2007) 4571–4581, https://doi.org/10.1002/chem.200601434.
[75] V. Shafirovich, A. Dourandin, W. Huang, N.E. Geacintov, The carbonate radical is a site-selective oxidizing agent of guanine in double-stranded oligonucleotides, J. Biol. Chem. 276 (27) (2001) 24621–24626, https://doi.org/10.1074/jbc.M101131200.
[76] E.V. Bakhmutova-Albert, H. Yao, D.E. Denevan, D.E. Richardson, Kinetics and mechanism of peroxymonocarbonate formation, Inorg. Chem. 49 (24) (2010) 11287–11296, https://doi.org/10.1021/ic1007389.
[77] X. Yang, Y. Duan, J. Wang, H. Wang, H. Liu, D.L. Sedlak, The impact of peroxymonocarbonate (HCO4-) on the transformation of organic contaminants during hydrogen peroxide (H2O2) *in situ* chemical oxidation (ISCO), Environ. Sci. Technol. Lett. 6 (12) (2019) 781–786, https://doi.org/10.1021/acs.estlett.9b00682.
[78] K. Nishikura, A-to-I editing of coding and non-coding RNAs by ADARs, Nat. Rev. Mol. Cell Biol. 17 (2016) 83–96, https://doi.org/10.1038/nrm.2015.4.
[79] M. Moreno-Villanueva, M. Wong, T. Lu, Y. Zhang, H. Wu, Interplay of space radiation and microgravity in DNA damage and DNA damage response, NPJ microgravity 3 (2017) 14, https://doi.org/10.1038/s41526-017-0019-7.